Phenotypic heterogeneity as key factor for growth and survival under oligotrophic conditions

Kankana Kundu [1,2]* **Nina Weber,**[1]
Christian Griebler [1,3] **and Martin Elsner** [1,4]

[1]*Institute of Groundwater Ecology, Helmholtz Zentrum Munchen, Ingolstadter Landstraße 1, 85764 Neuherberg, Bavaria, Germany.*
[2]*Center for Microbial Ecology and Technology (CMET), Ghent University, Coupure Links 653, Ghent 9000, Belgium.*
[3]*Division of Limnology, University of Vienna, Department of Functional and Evolutionary Ecology, Althanstrasse 14, Vienna, 1090, Austria.*
[4]*Chair of Analytical Chemistry and Water Chemistry, Technical University of Munich, Marchioninistrasse 17, D-81377 Munich, Germany.*

Summary

Productivity-poor oligotrophic environments are plentiful on earth. Yet it is not well understood how organisms maintain population sizes under these extreme conditions. Most scenarios consider the adaptation of a single microorganism (isogenic) at the cellular level, which increases their fitness in such an environment. However, in oligotrophic environments, the adaptation of microorganisms at population level – that is, the ability of living cells to differentiate into subtypes with specialized attributes leading to the coexistence of different phenotypes in isogenic populations – remains a little-explored area of microbiology research. In this study, we performed experiments to demonstrate that an isogenic population differentiated to two subpopulations under low energy-flux in chemostats. Fluorescence cytometry and turnover rates revealed that these subpopulations differ in their nucleic acid content and metabolic activity. A mechanistic modelling framework for the dynamic adaptation of microorganisms with the consideration of their ability to switch between different phenotypes was experimentally calibrated and validated. Simulation of hypothetical scenarios suggests that responsive diversification upon a change in energy availability offers a competitive advantage over homogenous adaptation for maintaining viability and metabolic activity with time.

Introduction

In many natural environments, heterotrophic bacterial growth and viability are limited by low availability of energy – carbon, and/or nutrients such as nitrogen and phosphorus (Egli, 2010; Hoehler and Jørgensen, 2013; Lever et al., 2015). These productivity-poor environments, the so-called oligotrophic, impose a challenge to microorganisms in sustaining metabolic activity and population size. Prominent examples are groundwater ecosystems and the deep sea, where readily available dissolved carbon is in the $\mu g\ l^{-1}$ range (Egli, 2010; Arrieta et al., 2015). However, numerous microorganisms do exist in these aquatic environments, even though cells are small, and their number is in the range of 10^3–10^5 cells ml^{-1} (Griebler and Lueders, 2009; Egli, 2010). It is assumed that only a small fraction of these natural microbial communities remains in an actively growing state (Griebler et al., 2001; Lennon and Jones, 2011). So, a fundamental – yet still unresolved – question is how these many microorganisms survive and may even maintain population sizes in environments that provide marginal energy for cell propagation or even barely support the maintenance of basic cellular functions (Hoehler and Jørgensen, 2013; Lever et al., 2015).

Abundant evidence suggests that energy-starved cells may undergo several adaptations that confer fitness under long-term energy limitation (Wick et al., 2001; Ihssen and Egli, 2004; Franchini and Egli, 2006; Lever et al., 2015). Most commonly observed responses under energy limitation are changes in morphology (Rappé et al., 2002; Fida et al., 2013; Mellage et al., 2015), cellular composition such as DNA, RNA and proteins (Boylen and Mulks, 1978), expression of stress-related proteins (Holmquist and Kjelleberg, 1993; Hartke et al., 1998; Nair and Finkel, 2004) and shifts in metabolic pathways (Stouthamer et al., 1990; Wick et al., 2001; Franchini and Egli, 2006). All these studies readily scale the average cell behaviour to the cell population level, but still tend to overlook the possibility that an individual population might adapt to energy limitation by differentiating into subpopulations. Several studies indicated phenotypic heterogeneity in microbial species (Balaban et al., 2004; Acar et al., 2008; Losick and Desplan, 2008; Ackermann, 2015;

Kotte *et al.*, 2015). For example, an isogenic population (single strain) was observed to express multiple distinct phenotypes due to stochastic gene expression (Balaban *et al.*, 2004; Acar *et al.*, 2008; Losick and Desplan, 2008). Also a responsive mechanism for phenotypic heterogeneity in carbon metabolism in *Escherichia coli* (Losick and Desplan, 2008; Kotte *et al.*, 2015) and nitrogen metabolism in *Klebsiella oxytoca* (Schreiber *et al.*, 2016) has recently been demonstrated. Remarkably, the conceptual picture obtained from natural microbial communities in oligotrophic environments does convey the presence of different metabolic states – co-existence of cells growing, growing at extremely low rates, non-growing but metabolically active and being non-active dormant (Lebaron *et al.*, 2001a,b; Lennon and Jones, 2011; Bayer *et al.*, 2016). It is widely believed that the phylogenetic composition of populations with different metabolic states are different (Bernard *et al.*, 2000; Zubkov *et al.*, 2002; Schattenhofer *et al.*, 2011; Vila-Costa *et al.*, 2012). Taking into consideration phenotypic heterogeneity in a single strain and the different metabolic states observed in natural communities, however, we hypothesize that – under low-energy flux – an isogenic population could differentiate into two or more subpopulations maintaining a small fraction of relatively more active 'growing' cells while the remaining population would be in maintenance mode, hereafter referred as 'non-growing'. By maintaining such phenotypic heterogeneity in an energy-limited environment, an isogenic population would improve its fitness so that one fraction of the population is prepared for unforeseen environmental conditions. For example, 'growing' cells will respond quickly to sudden energy availability while 'non-growing' cells can withstand extreme low energy availability (Gray *et al.*, 2019). The relevant scenario, however – the adaptation of cells that face conditions of constant catabolic energy limitation – has hardly been explored yet. Experiments conducted in the past mainly captured the extreme scenario of no energy availability (Finkel and Kolter, 1999; Zinser and Kolter, 2000; 2004; Finkel, 2006), that is, a rapid change from growth to starvation, such as in the stationary phase of batch experiments resulting in dormant cells, often subsumed into conceptual models for environmental systems (Stolpovsky *et al.*, 2011; Wang *et al.*, 2014). In contrast, the scenario we refer to here is the harsh condition of a constant energy limitation that acts on active microbial communities and individual populations within these communities and which – according to our hypothesis – may stimulate these populations to differentiate into 'growing' and 'non-growing' subpopulations when energy flux becomes very low and consequently less favourable for growth. This would also be in line with the findings of Egli and others that microorganisms physiologically adapt at the cellular level (e.g. proteome state) to prepare themselves in time for the worst case, that is, conditions of

extremely low or no energy availability (Wick *et al.*, 2001; Ihssen and Egli, 2004; Franchini and Egli, 2006; Egli, 2010). In contrast, the experiments in batch cultivation focusing on stationary phase provide an understanding of the adaptation strategy for the worst-case scenario – dormancy – but fail to capture the response of a population in a transition from high to low energy flux.

The aim of our study was, first, to explore the physiological and morphological adaptation of an environmentally relevant microorganism growing on low concentrations of carbon and nitrogen (sub-µM range) using appropriate staining assays and flow cytometry. For this purpose, *Arthrobacter aurescens* TC1 was grown on atrazine – a well-known micropollutant in aquatic environments – that acted as limiting nutrient source (both C and N). Initially, we investigated to what extent the population of *A. aurescens* TC1 exhibited signs of differentiation when atrazine supply was changed from high energy conditions (batch experiments) to medium energy flux (fed-batch experiments) by following the heterogeneity (growing and non-growing cells) in the population after each cell division. Later, chemostat experiments were performed to study the population adaptation along with long-term exposure to constant low energy availability by observing the difference in the nucleic acid content of the cells. The chemostats were also operated with biomass retention, that is, in retentostat mode. Biomass retention leads to a high cell density, which results in very low residual concentrations mimicking extremely low energy availability for the population. To verify our observation, the adaptation of another environmentally relevant bacterial strain – *Arthrobacter chlorophenolicus* A6 – was also studied in chemostat experiments. Second, based on our experimental observations, we bring forward a new mathematical modelling framework. In contrast to existing models (Pirt, 1982; Heijnen, 1999; Trautwein *et al.*, 2012), we included responsive differentiation into isogenic phenotypes resulting in population heterogeneity. The model can account for subpopulation dynamics as observed in chemostat experiments with consideration of repetitive and bidirectional transitions between different phenotypes. The potential advantage of microbial population differentiation was assessed and predicted for different hypothetical scenarios representing ecological challenges that microorganisms face under oligotrophic conditions. Our model framework therefore bridges the gap between chemostat and ecosystem models.

Results and discussion

Dynamic adaptation at population level under different energy fluxes

In batch and fed-batch experiments, cell proliferation of *A. aurescens* TC1 was monitored by cell membrane

staining. In principle, as the cell membrane is stained, each cell's fluorescent intensity is halved with every cell division. Hence, actively growing cells will be having low fluorescence, while non-growing cells retain high fluorescence. This allowed tracking the proliferation or growth of individual cells or subpopulations. A bimodal distribution of 'growing' versus 'non-growing' cells within the populations was observed (Fig. 1). In detail, the fluorescence pattern in flow cytometric measurements of samples collected at multiple time points exhibited three times higher (18% ± 4%) proportion of non-growing cells in fed-batch cultivation of *A. aurescens* TC1 compared to energy excess in batch (6% ± 3%). Live/dead staining

showed that this 'non-growing' fraction consisted of viable cells in both cases (Fig. 1). Active degradation of atrazine was observed in both batch and fed-batch experiments with residual atrazine concentrations of $2 ± 0.8$ mg l^{-1} and $200 ± 50$ µg l^{-1} (72 h), respectively. Artefacts such as a possible influence of pre-existing heterogeneity with a constant fraction of 'non-growing' cells or that the 'growing' subpopulations that increase in abundance in nutrient-rich conditions can be excluded. In that case, a constant number (cells ml^{-1}) of 'non-growing' cells would be expected under both conditions as both experiments were started with the same inoculum. Here, a 1.5 times higher number of 'non-
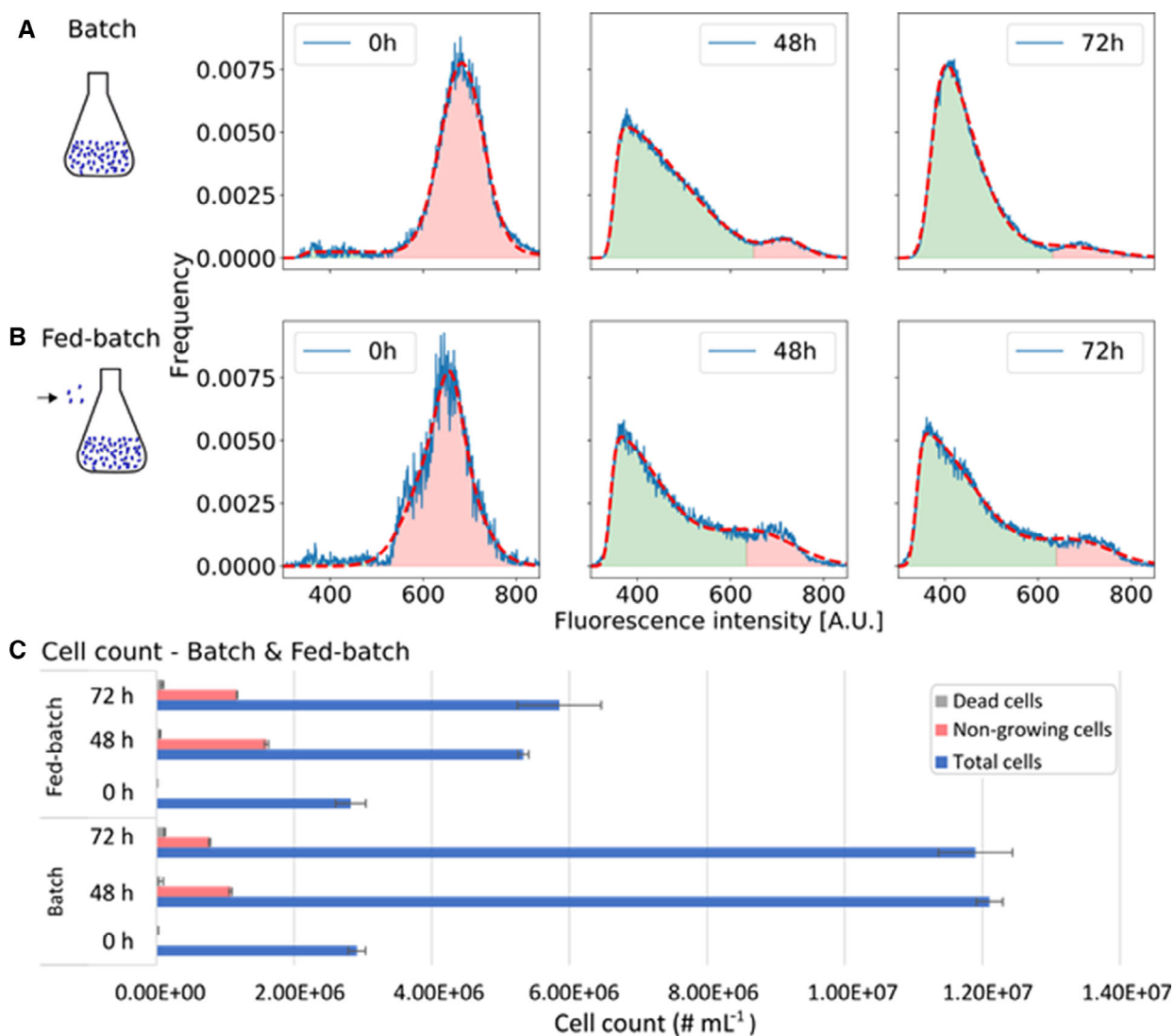
Fig 1. Heterogeneous adaptation of *Arthrobacter aurescens* TC1 cells with time under different energy fluxes. The areas of two subclasses of the population were calculated by determining the minima between the two prominent peaks in the distributions.
A. Batch experiment with high energy condition (atrazine concentration of 30 mg l^{-1}).
B. Fed-batch experiment with medium energy condition (atrazine supply rate of 0.16 mg h^{-1}).
C. Cell counts during batch and fed-batch experiments. Data points represent the average of samples and error bars indicate standard error ($n = 2$).

growing' cells (cells ml^{-1}) was observed in fed-batch than in batch.

Overall, the results from fed-batch and batch experiments demonstrated a heterogeneous adaptation of the cells to a change in energy availability – that is, only part of the cells resumes growth – but the results did not yet allow to follow temporally resolved adaptation steps. First, it cannot reveal the possible stochasticity in adaptation since cells which grew in the early phase of the experiment and switched to 'non-growing' later could still be in the low fluorescence intensity area as 'growing' cells. Second, after a certain number of cell divisions, the cell-specific fluorescence decreases so much that it is impossible to observe whether a synchronous population is established in the end. Hence, as a next step, the existence of multiple phenotypes at a condition of constant and long-term low energy availability in chemostat cultivation was explored.

Phenotypic heterogeneity influencing dynamics and steady-state population level in chemostats under different energy availabilities

Chemostat cultivation of *A. aurescens* TC1 at all dilution rates (*D*) resulted in a steady-state residual substrate concentration in the range of 80–420 μg l^{-1} (Supporting Information Table S1). The biomass or total cell concentration did not increase significantly (2.1–2.69 × 10^7 cells ml^{-1}, Supporting Information Table S1) at higher $D \geq \frac{\mu_{max}}{2}$ (0.068, 0.056 and 0.048 h^{-1}) compared to lower *D* (0.032 and 0.023 h^{-1}). Similar to the cell membrane staining in the fed-batch and batch experiment, total cell count after SYBR Green I staining revealed the progressive development of a subpopulation of cells with low nucleic acid (LNA) content at low *D* (Fig. 2A). Contrary to the earlier batch experiments that relied on cell membrane staining whose intensity was proportional to the number of cell divisions, the fluorescence intensity recorded here directly relates to the molecular composition of the cells – the total nucleic acid content [double-stranded (ds) DNA, single-stranded (ss) DNA, RNA] which is closely linked to the cells' physiological state or its gene expression phenotype (Neidhardt *et al*., 1990; Bremer and Dennis, 1996; Klumpp *et al*., 2009; Boer *et al*., 2010). The physiological state of the cells is reflected in the downstream phenotype such as growth which is mirrored in the nucleic acid content as growing cells have a higher gene and plasmid copy number, RNA, than the cells with low or no growth (Cooper and Helmstetter, 1968; Akerlund *et al*., 1995; Bremer and Dennis, 1996; Boer *et al*., 2010; Roller *et al*., 2016). Hence, high nucleic acid (HNA) and LNA cells detected by SYBR Green I staining correspond to two different phenotypes. Although we did not look at individual cell populations, the proteome analysis of the HNA-dominated cell population revealed significantly higher abundance of many proteins in compared to LNA-dominated one in retentostat (Kundu *et al*., 2019). This might indicate a differential gene expression, which in turn gives a hint of difference in DNA and RNA content of the HNA and LNA cells. The distribution of cells in LNA and HNA populations is a general characteristic of natural microbial communities (Gasol *et al*., 1999; Lebaron *et al*., 2001a,b; Sherr *et al*., 2006; Bouvier *et al*., 2007; Prest *et al*., 2013). As a general pattern, HNA subgroups are composed of more active and growing cells, whereas LNA populations contain cells with a low activity that are likely to be slow or non-growing (Li *et al*., 1995; Gasol *et al*., 1999; Lebaron *et al*., 2001a,b; 2002; Servais *et al*., 2003). Exceptions are a few taxa that cluster in LNA subgroups despite relatively high metabolic activity (Zubkov *et al*., 2001; Wang *et al*., 2009; Proctor *et al*., 2018). To explore whether LNA cells indeed represented a phenotype of 'non-growing', retentostat experiments were performed. Retentostat experiments provide a unique condition of extremely low (near-zero) growth rates and low substrate concentrations. This is achieved by the full retention of biomass. As substrate is still constantly supplied, cells initially continue to grow under these conditions. As a consequence, the amount of substrate per bacterial cell decreases with time. At a certain point, the amount of energy available becomes equal to the energy required for maintaining basic cellular functions. Hence, substrate addition does not provide sufficient resources for growth anymore, and cells inevitably remain in an active but 'non-growing' state. Retentostat cultivation has been recognized to create a 'twilight' between growth and stationary phase (Ercan *et al*., 2015). When cell concentration reached the plateau phase ('non-growing' phase) in our experiments, the flow-cytometry analysis revealed that the population was dominated by LNA cells – confirming that the LNA cells belonged to a 'non-growing' phenotype (Fig. 2B). As atrazine was nevertheless continuously degraded (the inflow concentration of 30 mg l^{-1} decreased to 10 ± 5 μg l^{-1} in the retentostat), this confirms that LNA cells were still active in substrate utilization. Active substrate utilization by 'non-growing' cells puts them apart from dormant cells as the later completely shutdown their metabolism and do not utilize substrate any more (Hoehler and Jørgensen, 2013; Sekhar *et al*., 2016). In this study, the HNA subpopulation increased with higher metabolic activity as measured in the form of a specific substrate (atrazine) conversion rate at higher *D*, whereas the LNA subpopulation dominated in retentostats, which showed less metabolic activity and no growth (Fig. 2C, Supplementary Information Table S1). Thus, we obtained evidence that the phenotypic heterogeneity
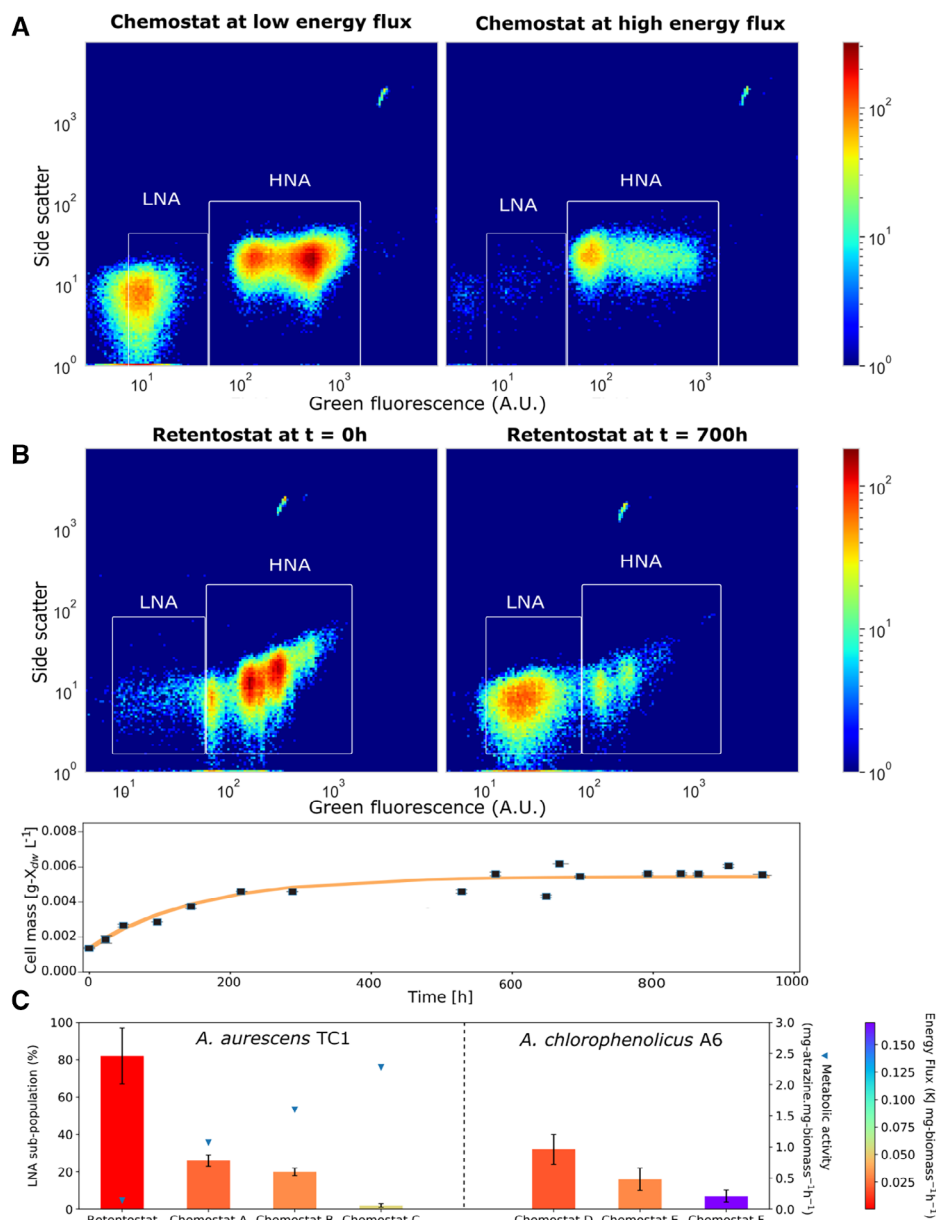
Fig 2. Long-term exposure to specific energy fluxes leads to differentiation into two phenotypes – a growing and a non-growing population where the non-growing fraction decreases with increasing energy availability.

A. Cytogram of green fluorescence versus side scatter for the steady-state population in chemostats revealed two cell types with different fluorescent intensity. Cells displaying a pronounced region of low fluorescence intensity are characterized by a low nucleic acid (LNA) content indicative of non-growers (D = 0.023 h^{-1}, 0.02 KJ mg biomass $^{-1}$ h^{-1} in the cultivation of *Arthrobacter aurescens* TC1, left), whereas high nucleic acid (HNA) cells are considered fast growers (D = 0.056 h^{-1}, 0.06 KJ mg biomass $^{-1}$ h^{-1} in the cultivation of *A. aurescens* TC1, right). The data are presented in a density plot where the shade of the colour is proportional to the points in each area.

B. Retentostat experiment, that is, chemostat with 100% biomass retention, shows HNA dominated population at the beginning of the cultivation later switched to LNA-dominated one at the end of cultivation.

C. Plot of percentage of LNA subpopulation derived in dependence on energy fluxes in chemostats and retentostats. Two bacterial strains – *A. aurescens* TC1 and *A. chlorophenolicus* A6 were grown on atrazine and 4-chlorophenol, respectively, in chemostats and retentostats at different dilution rates. Metabolic activity of *A. aurescens* TC1 cells are shown as specific substrate (i.e. atrazine) consumption rate (mg-atrazine mg-biomass^{-1} h^{-1}). Chemostat A, B, C represents the cultivation of *A. aurescens* TC1 at dilution rates of 0.023, 0.032, and 0.056 h^{-1}, respectively. Chemostat D, E, F represents the cultivation of *A. chlorophenolicus* A6 at dilution rates of 0.015, 0.022, and 0.081 h^{-1} respectively. Data points represent the average of samples, and error bars indicate standard error (n = 2).

characterized by subpopulations of HNA and LNA content was related to functional differences between the two subpopulations.

The capability of one genotype (individual strain) to alter its phenotypic state or activity (e.g. metabolism) in response to external environmental stimuli – phenotypic

plasticity – is a well-known phenomenon (Garland and Kelly, 2006; Kelly *et al*., 2011). Interestingly, here the isogenic population was not observed to adapt its activity or physiological state synchronously but instead underwent differentiation (or diversification) into multiple phenotypes at a given time under the natural selection pressure from limited energy availability. To exclude that this heterogeneity was specific to *A. aurescens* TC1, another strain – *A. chlorophenolicus* A6 – was cultivated in a chemostat under the same operating conditions but with 4-chlorophenol instead of atrazine as sole carbon and energy source. Indeed, observations with *A. chlorophenolicus* A6 were similar to *A. aurescens* TC1: while initially, HNA cells dominated, a subpopulation of LNA cells emerged that increased in importance with decreasing energy availability (Fig. 2C). Phenotypic heterogeneity is often observed in nature upon large variations in environmental conditions when sensing environmental cues and responding accordingly by changing gene expression may not always be possible (Acar *et al*., 2008; Ackermann, 2015). Hence, as a protective feature for survival, individual strains can express phenotypic variants without even sensing environmental cues – a strategy known as 'bet-hedging' (Philippi and Seger, 1989; Ackermann, 2015). Remarkably, in this study, phenotypic heterogeneity, that is, heterogeneous adaptation, was observed at steady-state conditions when at least 5–6 hydraulic retention times had passed. This time span provided ample opportunity to the cells for sensing external environmental conditions, adapting accordingly, and establishing a synchronous population fit for the specific circumstance. Hence, the detection of LNA and HNA cells in chemostats indicates that phenotypic heterogeneity also enters the picture when energy flux remains steady but is small and insufficient to sustain growth and metabolic activity of the entire population so that it should not solely be considered as an outcome of 'bet-hedging'.

Since chemostat cultivation represents a stable system with a constant residual substrate concentration over time, this raises the question for the origin of the observed variation in the intracellular concentration of macromolecules at the single-cell level. A well-recognized factor in *E. coli* is stochasticity in gene expression within individual cells (Elowitz *et al*., 2002; Raser and O'shea, 2005; Acar *et al*., 2008; Ackermann, 2015). Other reasons contributing to phenotypic heterogeneity are different timers controlling cell division (Nishimura and Bailey, 1981; Raser and O'shea, 2005) and cellular memory (Losick and Desplan, 2008). Microorganisms also employ specific mechanism for differentiating into subpopulation with resistance against certain antibiotics (Balaban *et al*., 2004). An intra-cellular metabolite flux sensor was suggested as a trigger for the switch into a different phenotype with

respect to the central carbon metabolism in *E. coli* (Kotte *et al*., 2015). In the case of *A. aurescens* TC1 a mechanism must also exist by which one phenotype is transformed into the other to justify the observation of both HNA and LNA cells, in particular in chemostats under continuous biomass washout. Hence, a continuous switch of cells between the putative 'growing' – HNA and 'non-growing' – LNA state is required. In retentostat experiments, initially, an HNA-dominated population prevailed, which later changed to an LNA-dominated population, providing a second line of evidence of active switching. Exploring the mechanism by which *A. aurescens* TC1 diversifies into two phenotypes is beyond the scope of this study. Nevertheless, the increased fraction of 'non-growing' cells at low substrate loads (low *D*) in a chemostats and retentostats indicates that the amount of available catabolic energy is a potential trigger for such a phenotypic switch. It has been previously suggested by cytometric analysis of microbial communities from various aquatic habitats that there is a possibility of dynamic exchanges between the LNA and HNA cells (Servais *et al*., 2003; Bouvier *et al*., 2007). Recently, both cytometric analysis and 16S rRNA sequencing data showed that individual operational taxonomic units were well represented in both LNA and HNA groups (Rubbens *et al*., 2019). Hence, our results are consistent with these observations and, for the first time, provide experimental evidence of phenotypic heterogeneity characterized by HNA and LNA cells in the isogenic population – of a continuous switch between these two subpopulations as a way of adaptation to constant low energy availability. In the following section, a mechanistic model-based analysis of microbial physiological states is brought forward to capture the population heterogeneity in microbiallydriven processes.

Model construction and analysis

Based on our hypothesis that two subpopulations emerge under constant low energy flux, a conceptual framework for model-based analysis of population dynamics towards heterogeneous adaptation in chemostats was developed (Fig. 3 and Eqs 1–11). The proposed model extended currently available frameworks in the literature (Jones and Lennon, 2010; Wang *et al*., 2014) to capture the essential microbial system dynamics towards differences in energy availability. The model framework (i) is based on the concept of a 'non-growing' state which represents the 'twilight' between growth and dormancy; (ii) accounts for a low substrate consumption by non-growing cells for maintenance purpose, which is a notable advancement compared to the models based on dormancy where no substrate is consumed by dormant cells (Jones and Lennon, 2010; Wang *et al*., 2014); and (iii) follows an energy availability-driven approach to consider the
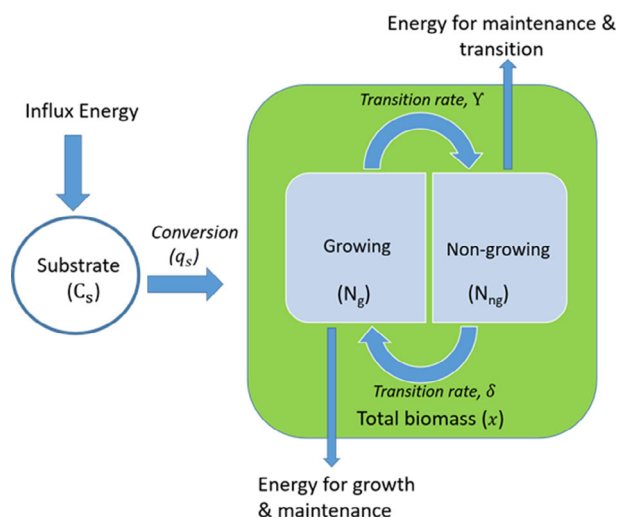
Fig 3. Schematic representation of the proposed modelling approach for the simulation of two subpopulations with different physiological states. [Color figure can be viewed at wileyonlinelibrary.com]

bidirectional and repeatable transition between 'growing' and 'non-growing' states.

Population dynamics in chemostats

If total biomass (x) is composed of a growing (N_g) and a non-growing N_{ng} population as observed in the experiments, the dynamics of subpopulations N_g and N_{ng} can be described using Eqs 1 and 2, respectively.

$$\frac{dN_g}{dt} = \mu_g . N_g - D \cdot N_g - K = \frac{\mu_{max} \cdot C_s}{K_S + C_s} \cdot N_g - D \cdot N_g - K, \qquad (1)$$

$$\frac{dN_{ng}}{dt} = -D . N_g + K, \qquad (2)$$

where K denotes the transition rate from the growing, N_g to the non-growing state, N_{ng}, μ_g is the specific growth rate of growing population, μ_{max} corresponds to maximum specific growth rate, K_S corresponds to Monod affinity constant and D is the dilution rate.

The transition rate between growing and non-growing state was expressed in terms of the relative growth rate, that is, the ratio of specific growth rate, μ to maximum specific growth rate, μ_{max}, by the following expression adopted from Konopka (1999).

$$K = \left(1 - \frac{\mu_g}{\mu_{max}}\right) \cdot \Upsilon \cdot N_g - \left(\frac{\mu_g}{\mu_{max}}\right) \cdot \delta \cdot N_{ng}, \qquad (3)$$

where Υ represents the first order rate constant for a transition of growing cells to non-growing cells and δ is the first-order rate constant for the vice versa case. When

Monod kinetics, that is, $\mu = \frac{\mu_{max} \cdot C_s}{K_S + C_s}$ is applied to describe the microbial growth, regulation of growth and hence transition occurs via substrate availability, which is controlled by D. By considering (μ/μ_{max}), the substrate saturation level which is formulated by $\frac{C_s}{K_S + C_s}$, composed of substrate concentration and the Monod affinity constant serves as a switch function for 'growing' to 'non-growing' and vice versa. At a high D, $C_s \gg K_S$ and $\mu \approx \mu_{max}$, and the population will be comprised of only 'growing' cells and when $C_s \ll K_S$ or $C_s \approx K_S$, the heterogeneity of the population is established.

A change from continuous feeding to intermittent feeding results in a potential starvation condition. To capture this phenomenon, the endogenous decay rates K_{d1} and K_{d2} for both N_g and N_{ng} the subpopulation are introduced, respectively, and Eqs 1 and 2 are modified as

$$\frac{dN_g}{dt} = \mu_g \cdot N_g - D \cdot N_g - K - \theta(C_s) \cdot K_{d1} \cdot N_g, \qquad (4)$$

$$\frac{dN_{ng}}{dt} = -D \cdot N_{ng} + K - \theta(C_s) \cdot K_{d2} \cdot N_{ng}. \qquad (5)$$

A Dirac-delta step function was used for activation of K_d based on C_s such that

$$\theta(C_s) = \begin{pmatrix} 1, C_s \to 0 \\ 0, C_s > 0 \end{pmatrix}. \qquad (6)$$

This function ensures that the cell's maintenance demand is either taken into account by K_d or by m_s (see below) so that double accounting is avoided.

Dynamic and residual substrate concentration under heterogeneous adaptation

We observed that the non-growing cells utilize the substrate to require energy for maintaining vital cell functions and survival. Hence, the maintenance demand of 'growing' and 'non-growing' fraction, m_s and m'_s, respectively, are introduced in the residual substrate (C_s) equation, represented as

$$\frac{dC_s}{dt} = D \cdot (C_{s0} - C_s) - \mu_g \cdot \frac{N_g}{Y_G} - m_s \cdot N_g - m'_s \cdot N_{ng}$$
$$- \frac{\mu_g}{\mu_{max}} \cdot \delta \cdot N_{ng} \cdot \psi, \qquad (7)$$

where Y_G denotes the (hypothetical) maximum growth yield, and ψ is specific substrate consumption rate during a switch from 'non-growing' to 'growing'.

Introducing a growing fraction of biomass, $\alpha = \frac{N_g}{x}$, Eq. 7 can be reformulated as

$$\frac{dC_s}{dt} = D \cdot (C_{s0} - C_s) - \mu_g \cdot \alpha \cdot \frac{x}{Y_G} - m_s \cdot \alpha x - m'_s (1-\alpha) x$$
$$- \frac{\mu_g}{\mu_{max}} \cdot \delta \cdot (1-\alpha) x \cdot \psi. \tag{8}$$

At steady state, $\frac{dC_s}{dt} = 0$ and if the consumption rate $q_s = \frac{D \cdot (C_{s0} - C_s)}{x}$ is described by a Michaelis–Menten type expression

$$q_s = \frac{q_s^{max} \cdot C_s}{K_s + C_s}, \tag{9}$$

where K_s and q_s^{max} are Monod affinity constant and maximal substrate consumption rate, the residual substrate concentration can be given by the following equation:

$$C_s = \frac{K_S \cdot \xi}{q_s^{max} - \xi}, \tag{10}$$

where

$$\xi = \frac{\alpha \cdot \mu_g}{Y_G} + m_s \cdot \alpha + m'_s \cdot (1-\alpha) + \frac{\mu_g}{\mu_{max}} \cdot \delta \cdot (1-\alpha) \cdot \psi. \tag{11}$$

In the case of homogenous adaptations in chemostats, K becomes zero and simultaneously, all the terms associated with N_{ng} becomes zero.

Model verification using chemostat experiment data at different dilution rates

The parameters Υ, δ and ψ could be determined with a high confidence (coefficient of variation < 5%) by using the experimental data set at D of 0.023 h^{-1}. The calibrated model parameter values are listed in Table 1. The estimated rate constants (δ and ψ) indicate that 'growing' cells employ a fast-switching strategy whereas 'non-growing' cells are slow-switching. Subsequently, the calibrated model (D = 0.023 h^{-1}, Eqs 1, 2 and 7) was used to simulate N_g, N_{ng} and C_s concentrations at higher dilution rates up to 0.068 h^{-1}. When compared with the experimental data, a very good agreement between experiment and simulation was obtained (Fig. 4). This indicates that Υ, δ and ψ values in the present model framework are insensitive to the change in D, and the model is well capable of capturing the (sub) population and substrate dynamics at varying chemostat conditions.

Effect of parameter uncertainty and global sensitivity analysis

For the parameter uncertainty analysis on model output, C_s, N_g and N_{ng} by Markov Chain Monte Carlo (MCMC) technique, the optimal parameter set (Table 1) was used as starting position to stay close to the region where the likelihood is expected to be cantered and a uniform prior on each parameter in a physically applicable range was applied. Supporting Information Fig. S1 shows the traces of MCMC chain analysis through 350,0000 iterations. As there was no apparent drift observed, MCMC converged, suggesting that the parameters were identifiable at these conditions. The projections of the nine-dimensional likelihood into one- and two-dimensional marginal distributions are shown in Supporting Information Fig. S2. The two-dimensional projections show very little covariance

Table 1. Values of kinetic parameters used for the simulation of 'growing', 'non-growing' cells and residual substrate concentration.

Kinetic parameters	Units	Definition	Values
μ_{max} [a]	h^{-1}	Maximum specific growth rate	0.11 ± 0.02
K_S [a]	µg l^{-1}	Monod affinity constant	237 ± 57
q_s^{max} [a]	Gram substrate per gram biomass per hour (g-S g-X^{-1} h^{-1})	Maximum substrate consumption rate	4.08 ± 5.1e-1
m_s [a]	Gram substrate per gram biomass per hour (g-S g-X^{-1} h^{-1})	Maintenance demand for growing fraction	0.22 ± 5.0e-2
m'_s	Gram substrate per gram biomass per hour (g-S g-X^{-1} h^{-1})	Maintenance demand for non-growing fraction	0.10 ± 4.0e-3
Y_G	Gram biomass produced per gram substrate (g-X g-S^{-1})	Maximum growth yield	0.028 ± 1.0e-3
Υ	h^{-1}	Rate constant for transition from growing to non-growing fraction	0.006 ± 1.0e-5
δ	h^{-1}	Rate constant for transition from non-growing to growing fraction	0.002 ± 1.0e-4
ψ	Gram substrate per gram biomass per hour (g-S g-X^{-1} h^{-1})	Substrate consumption rate during a switch from non-growing to growing	0.028 ± 3.0e-3
K_{d1} [b]	h^{-1}	Endogenous metabolism rate for growing fraction	0.006 ± 1.0e-3
K_{d2} [b]	h^{-1}	Endogenous metabolism rate for non-growing fraction	0.002 ± 1.0e-3

[a]From Kundu *et al.* (2019).
[b]Calculated according to $K_d = m_s \lor m'_s \cdot Y_G$.
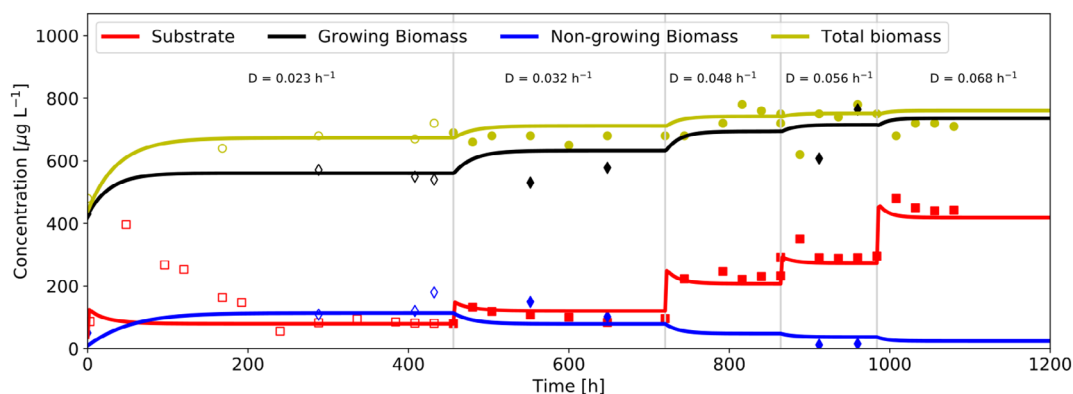
Fig 4. Dynamic total biomass, 'growing' (HNA) and 'non-growing' (LNA) biomass, and substrate, atrazine concentration in the chemostats under varying energy flux controlled by dilution rates.
Solid lines depict the model prediction (Eqs 1, 2 and 7), whereas the markers show the experimental data (unfilled markers indicate data points used for model calibration). Data are from one biological replicate. The data for the second biological replicate is provided in Supporting Information (Fig.S5, Data S1).

among any two parameters, and the marginal distribution histograms (along the diagonal) are nicely peaked. The constraints on the parameters are consistent with the pre-estimated values. Thus, the parameter uncertainty was negligible in this study, and a minor impact on the model result is expected.

For the sensitivity analysis (SA), the ranges of all tested parameters are listed in Supporting Information Table S2. Variance-based global SA indicates that C_s is most sensitive to the model parameters q_s^{max}, K_S, Y_G and α (Fig. 5A). Moreover, α, which is the growing fraction of biomass, is most influenced by Υ, δ (Fig. 5B and Supporting Information Fig. S3). This supports earlier observations that the transition rate between different phenotypes has an impact on population heterogeneity (Acar *et al*., 2008). For example, if the transition between phenotypic states is much faster than the transition between the two environmental conditions, a high level of population heterogeneity is established. Although not at the same condition of constant low energy flux, Balaban *et al*., 2004 measured the transition rate from 'growing' to 'non-growing' states in batch experiment, which is 10 times higher than our estimated value. Some studies focused on the response of starvation on metabolic activity of the population (Albertson *et al*., 1990; Kjelleberg *et al*., 1993; Konopka *et al*., 1996). A transition rate of $0.2\,h^{-1}$ was found to fit the observation of Carbon-starved marine bacteria – *Vibrio* sp. S14 – when it switches from active to non-active cells (Kjelleberg *et al*., 1993; Konopka, 1999). The time required for inactive cells to resume growth is dependent on the physiological adaptation of the cells under starvation and can be as long as $200\,h$ (Albertson *et al*., 1990). In case of cells with a near-zero growth rate, a lag period of $2–7\,h$ upon substrate upshift was observed (Konopka *et al*., 1996). Hence, the

transition rates vary with organisms and are dependent upon the physiological state and the previous history of the cells. This is also reflected in our study, where *A. chlorophenolicus* showed a higher population heterogeneity at low energy availability than *A. aurescens* TC1 did (Fig.2).

Simulation results to demonstrate the benefit of two subpopulations in the environment

Hypothetical scenario 1: Constant low substrate availability – Heterogenous adaptation allows survival of active 'growing' cells at a minimum substrate concentration. Growing cells have a relatively high metabolic activity, and hence, their energy requirement for maintaining particular subcellular processes such as sustaining the proton motive force, osmoregulation, protein turnover, repair and so on known as maintenance energy is much higher than in 'non-growing' cells (Van Bodegom, 2007; Kempes *et al*., 2017; Kundu *et al*., 2019). The maintenance energy of 'non-growing' cells is dependent on their physiological adaptation (Morita, 1997; Lever *et al*., 2015). Hence in oligotrophic environments where the energy availability is extremely low and steady with time, the 'growing' cells continuously strive for energy sources to maintain their growth and viability, whereas 'non-growing' cells are challenged by their slow metabolism to acquire energy. To comprehend the advantage of a population's capability of entering in a reversible state of low activity and a state of 'non-growing', the composition of the population under a steady-state condition of a chemostat was simulated using Eq. 10 (Fig. 6). Two kinetic properties of the growing cells, K_s and q_s^{max}, were varied considering different substrate-dependent energy requirement to sustain growth and activity (as revealed
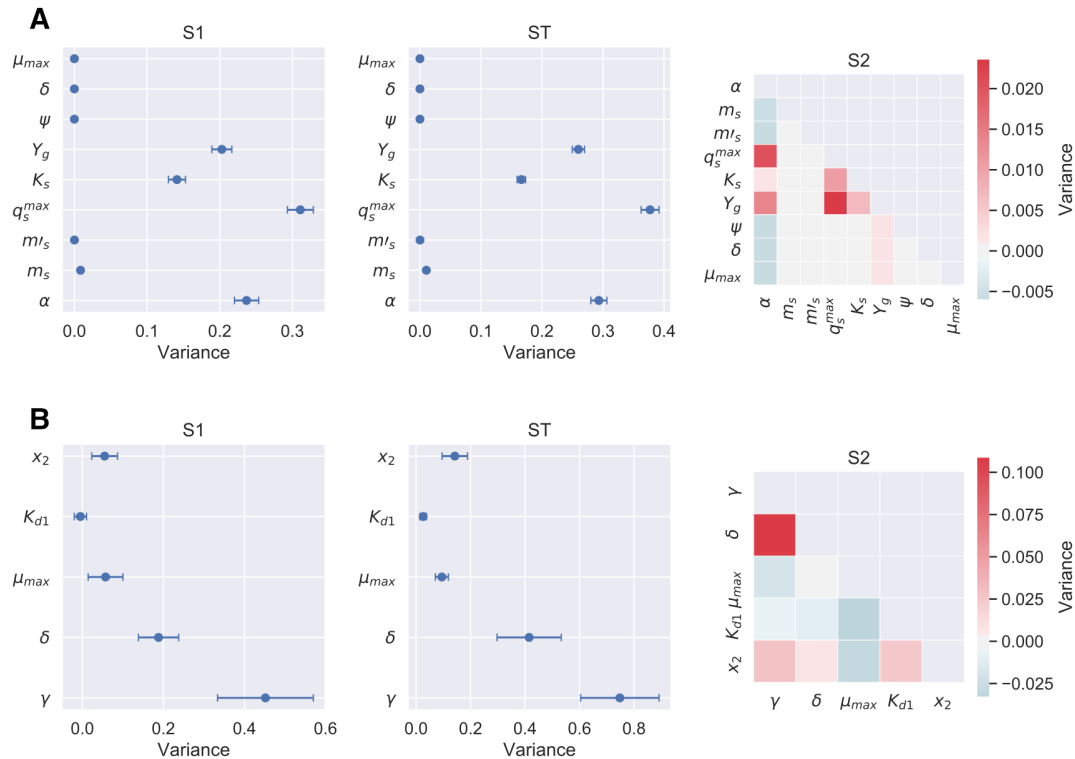
Fig 5. First order (S1), total order (ST) and second order (S2) Sobol' indices for all model parameters on residual substrate concentration (A) and on 'growing' cells (B) in a chemostat.
Most influential parameters have a higher variance. The error bar represents the confidence intervals based on 10,000 bootstrap samples.

by the most influential parameters, see above). The 'non-growing' subpopulation was classified into three categories based on their physiological state, hence, differing in maintenance requirement (m'_s). The simulation results show that the heterogeneous adaptation, which resulted in existence of both 'growing' and 'non-growing' cells allows maintenance of 'growing' cells at a much lower substrate concentration (Fig. 6). For example, a fraction of growing cells is maintained at a substrate concentration as low as 4 µg l^{-1}, while the minimum substrate concentration required for maintaining all cells in a highly active and growing state was in the range of 20–80 µg l^{-1}. The highest required substrate concentration, 80 µg l^{-1} was observed for growing cells of type II which had a low q_s^{max} and high K_s. For the growing cells (type III) with a low K_s and a high q_s^{max}, a three times higher fraction (0.6) of the cells were found to be in a 'growing' state at 4 µg l^{-1} than other types of growing cells. Although it would seem logical for the entire population to enter into a 'non-growing' state or even dormancy under sparse energy availability, the benefit of maintaining a fraction of dividing, highly active cell as observed experimentally seems to stem from the ability of active cells to more rapidly respond to even short-term pulses of energy (Lewis, 2007).

Hypothetical scenario 2: Fluctuations in energy availability – Heterogeneous adaptation leads to the higher richness in the population. To determine whether the population with the capacity to switch between 'growing' and 'non-growing' state would manifest a higher persistence through environmental fluctuations in terms of energy availability, a hypothetical microbial system comprised of two populations, was simulated. Both populations were supposed to be isogenic and to have similar growth and substrate utilization kinetics (μ_{max}, K_s and q_s^{max}). However, the first population was composed of only 'growing' cells with a fast metabolism and a high maintenance requirement (m_s). Whereas, the second population adapts heterogeneously, that is, differentiates, into 'growing' (characterized by the same kinetic parameters as the first population) and 'non-growing' cells with a low maintenance requirement (m'_s). The kinetic parameter values assigned to these two populations are listed in Table 1. The model simulation tested the competitive success of these two types when the populations were intermittently fed with substrate (30 mg l^{-1}) pulses of 5 h in 40 h intervals. Hence, 5 h of feeding represented the 'high energy flux' condition, whereas the 35 h of no feeding the 'starvation phase'. The composition of the population with the capability of
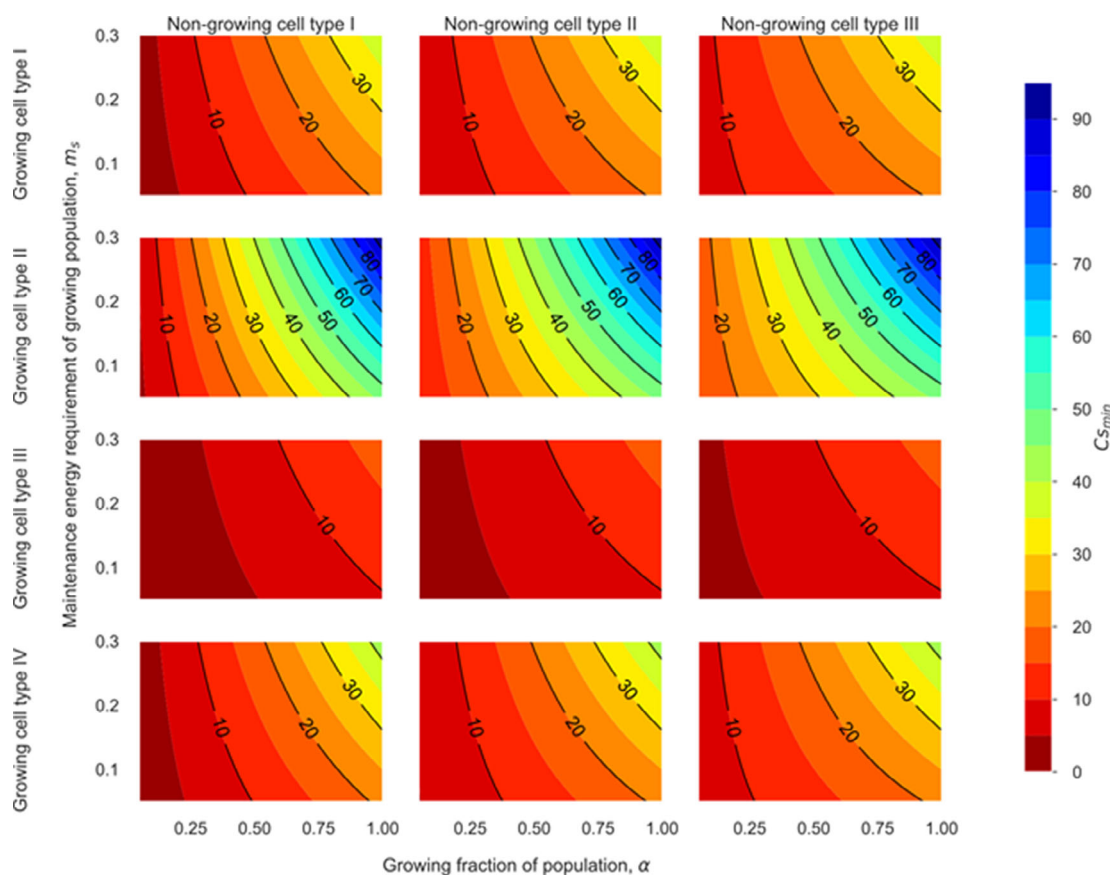
Fig 6. Prediction of substrate concentration co-existence of two subpopulation to variation in 'growing' fraction (α) with $\mu = 0.023$ h^{-1}, and maintenance demand (m_s) for different combinations of K_S, q_s^{max} and maintenance demand (m_s') of the 'non-growing' population (Eq. 10).
Growing cell type I, $K_S = 220$ µg l^{-1}, $q_s^{max} = 4$ g-S g-X^{-1} h^{-1}; growing cell type II, $K_S = 220$ µg l^{-1}, $q_s^{max} = 2$ g-S g-X^{-1} h^{-1}; growing cell type III, $K_S = 100$ µg l^{-1}, $q_s^{max} = 4$ g-S g-X^{-1} h^{-1}; growing cell type IV, $K_S = 100$ µg l^{-1}, $q_s^{max} = 2$ g-S g-X^{-1} h^{-1}. Non-growing cell types I, II and III has (m_s') of 0.02, 0.08 and 0.12 g-S g-X^{-1} h^{-1}.

heterogenous adaptation under this feeding condition was simulated using Eqs. 4, 5 and 8.

The simulation results for the intermittent feeding scenario showed that the total biomass was mainly comprised of 'growing' cells during pulse feeding and 'non-growing' cells dominated during the 'starvation phase' (Fig. 7A). After each supply event, the substrate concentration drops to zero, yielding a regular saw-tooth pattern that followed the substrate supply frequency. The population without the ability of heterogeneous adaptation showed the same saw-tooth pattern, but the total biomass was significantly less compared to that of a population with phenotypic differentiation (Fig. 7A). Hence, the heterogeneous adaptation prevented the significant loss of biomass and metabolic activity under resource limitation and provided a competitive advantage by the evolution of fit-for-purpose subpopulations under different environmental conditions.

In the previous feeding regime, the inflow rate was constant with intermittent breaks. However, in nature diurnal inflow rate variation in energy supply is also frequent. Hence, the response of two populations under a diurnal energy supply variation was induced as a sinusoidal variation in the feed flow rate given by the following function:

$$F(t) = 12 + 0.6 \times 12 \cdot \sin\left(\frac{2\pi}{(24)}t - \left(\frac{\pi}{5}\right)\right). \quad (12)$$

The abundance of growing cells exhibited regular variations in both the populations (Fig. 7B). Here, also, the total biomass of heterogeneous populations was higher than the population comprising of only 'growing' cells. In effect, the heterogenous adaptation favours maintaining population size under diurnal fluctuation in energy availability.

In the environment, in particular in surface or near-surface habitats, microbial communities face regular and irregular changes in environmental conditions at a variety of frequencies (e.g. from diurnal via seasonal to
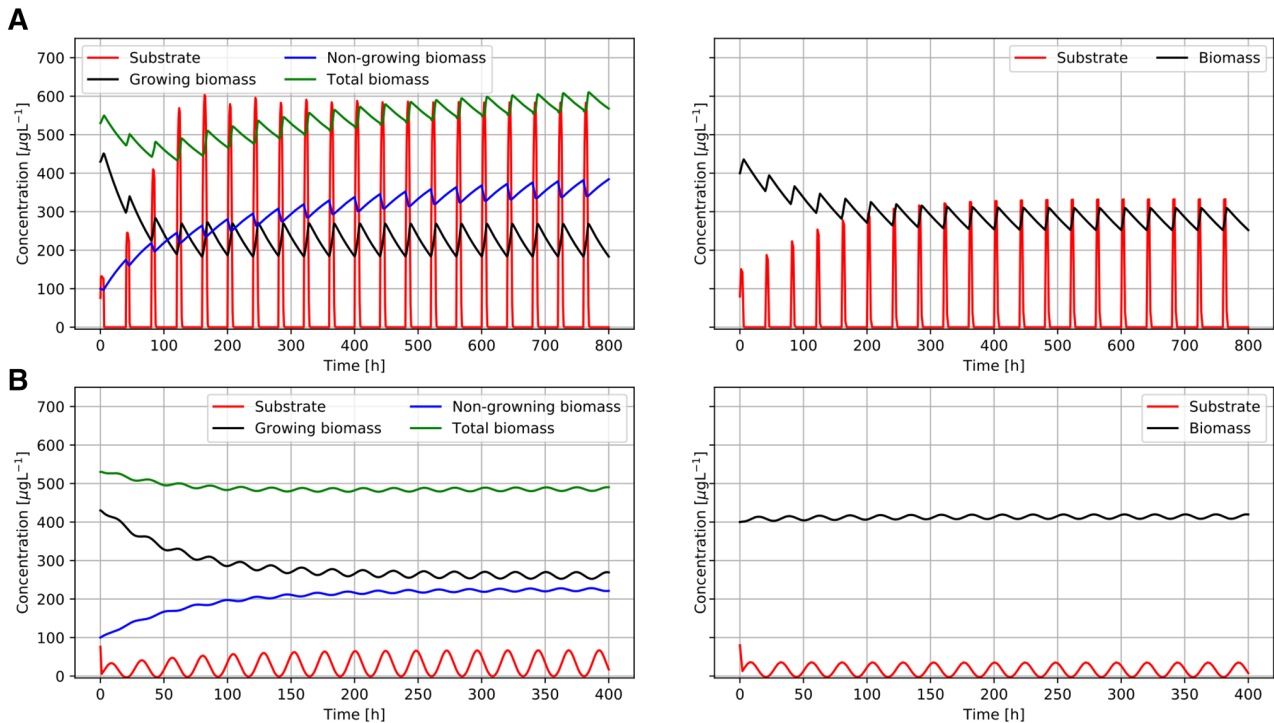
Fig 7. Response of a heterogeneous and homogenous population under (A) pulse feeding representing 'feast and famine' conditions in the environment and (B) sinusoidal feeding strategy representing diurnal energy supply variation in the environment (Eqs 4, 5 and 8).

interannual changes). According to the results presented in this study, these conditions promote not only the enduring co-existence of species differing in growth and non-growth strategies contributing to a high microbial richness and diversity but also subpopulations exhibiting variable metabolic activity. Specifically, we would expect intra-population differentiation among microbial species in energy-limited habitats such as groundwater or the deep sea. This study also provides a hint that degradation of pollutants at low concentrations might be catalysed by different subpopulations of the same microorganisms, and this differentiation into several subpopulations could potentially make active degradation possible at extremely low concentrations. Further studies focusing on the mechanism responsible for the switching phenomenon and the physiological characteristics of the subpopulations in several species for diverse compounds will highlight the specific adaptation strategies at the population level in a resource-limited environment and provide a base for constructing a population balance model for more complex environmental systems.

Experimental and model analysis procedures

Cultivation media and microbial strains

Arthrobacter aurescens TC1 (Strong *et al*., 2002) and *A. chlorophenolicus* A6 (Westerberg *et al*., 2000) were cultivated at 23–28°C in a mineral salt (MS) medium (Strong *et al*., 2002). The medium was prepared in MilliQ® water (Milli-Q® Integral Water Purification System, Millipore, Darmstadt, Germany), with a total organic carbon concentration of < 10 μg l^{-1}, and pH was adjusted to 7.2 with sodium hydroxide (1.0 M). After autoclaving at 121°C for 20 min, the medium was cooled and was supplemented with atrazine (Cfm Oskar Tropitzsch, Marktredwitz, Germany) as a sole C and N source for *A. aurescens* TC1 at 30 mg l^{-1} final concentration or with 4-chlorophenol (Merck, Darmstadt, Germany) as C source at 220 mg l^{-1} final concentration together with NH_4NO_3 (0.5 g l^{-1}) as N source for *A. chlorophenolicus* A6. Subsequently, filter-sterilized (0.22 μm) $FeCl_3 \cdot 6H_2O$ solution (5.14 mg l^{-1}) was added. To prepare the precultures for cultivation in bioreactors, *A. aurescens* TC1 and *A. chlorophenolicus* A6 were grown on MS media with excess atrazine and 4-chlorophenol (220 mg l^{-1}), respectively, in a shaken flask until an optical density (OD_{600}) of 0.1 was reached.

Batch, fed-batch and continuous cultivations

Experiments were performed in duplicate 3 l bioreactors (Applikon Biotechnologie B.V., Delft, The Netherlands) operated in batch, fed-batch, and continuous mode (chemostat). Bioreactors were equipped with pH, aeration, temperature, level and agitation controls by

myControl® (Applikon Biotechnologie B.V., Delft, The Netherlands). Cells from pre-cultures [10% (vol/vol)] were used for inoculation. For bioreactor operation, the agitation speed was set to 600 rpm, and dissolved oxygen was maintained at 50% of saturation. The pH was held constant at 7.2, and the temperature was 25°C. The bioreactors were protected from light. Four separate runs were performed for *A. aurescens* TC1. (i) Chemostat experiment: Two bioreactors were operated at D [defined as the ratio of the medium flow rate (ml h^{-1}) and culture volume (l)] of 0.023, 0.032, 0.056 and 0.068 h^{-1} for *A. aurescens* TC1. The volume of the chemostat was maintained at 2000 ml by a level controller. Dilution rates were progressively changed in the two reactors only after achieving a steady state at a particular D, meaning that culture parameters such as cell concentration and atrazine remained constant (< 5% and < 10% relative variation respectively) for at least five reactor volume changes. (ii) Retentostat experiment: Two bioreactors were freshly started and operated as retentostat, that is, in biomass retention mode at a dilution rate of 0.020 h^{-1}. Biomass retention was achieved by installing an autoclavable polyethersulfone cross-flow filter with a pore size of 0.22 μm (Flownamics, Madison, WI) via a head plate port to the bioreactors. An internal sterile filtration loop was established with a connection of the level sensor to the myControl® and a peristaltic pump to allow filtration of effluent during level control throughout the cultivation. The volume was kept constant at 2000 ml throughout the cultivation. (iii) Fed-batch experiments: Two bioreactors were operated in variable volume fed-batch mode with an initial volume of 1000 ml. Immediately after the inoculation, the feeding started with MS media containing atrazine (conc. 30 mg l^{-1}) at a flow rate of 0.09 mlmin^{-1}. (iv) Batch experiments: Two bioreactors were operated in batch mode with a volume of 1000 ml and atrazine conc. of 30 mg l^{-1}.

For 4-chlorophenol degradation with *A. chlorophenolicus* A6, the bioreactors were operated at D 0.01, 0.02 and 0.08 h^{-1} under the same operating conditions, with the exception that the working volume of the bioreactor was maintained at 1600 ml.

Cell staining and flow cytometry

For discrimination between growing and non-growing cells, PKH-67 – a fluorescent, cell membrane-intercalating dye was used to monitor cell proliferation by flow cytometry (Wallace *et al*., 2008) in batch and fed-batch experiments. *A. aurescens* TC1 cells were centrifuged for 4 min at 4000 g and 4°C. The cells were washed in ice-cold MS media before being centrifuged a second time. For staining, the cells were resuspended in 1 ml diluent buffer C (Sigma-Aldrich) to reach a final cell density of ∼2 × 10^7 cells ml^{-1}. A freshly prepared PKH-67 dye (Sigma-Aldrich) solution in diluent C (1 ml) was added to the cell suspension with a final dye concentration of 2 × 10^{-6} M. After 3 min of incubation with periodic gentle mixing in between, 2 ml of ice-cold MS media containing 1% (wt/vol) bovine serum albumin (Sigma-Aldrich) was added to stop the staining reaction. After further centrifugation, the supernatant was discarded, and the cells were washed twice before inoculation to the batch and fed-batch bioreactors. After 5–10 min of inoculation, the first samples were taken and used as a t_0 reference. Samples were immediately analysed in a Cytomics FC 500 flow cytometer (Beckmann Coulter, Krefeld, Germany) equipped with a laser with two different filters – 488 nm (40 mW) and 638 nm (25 mW). To further distinguish non-growing cells from dead cells, propidium iodide 10 μl ml^{-1} (0.5 mM stock solution, Invitrogen-Thermo Scientific, Waltham, MA) was used. The samples were incubated for 13 min at 37°C before adding reference beads (Trucount Tubes, Becton Dickinson, Franklin Lakes, NJ) for cell quantification (Bayer *et al*., 2016). The following parameters were used: discriminator FL2/1, forward scatter 276V/gain 1.0, side scatter 327V/gain 5.0, FL1 630/gain 1.0, FL2 (yellow fluorescence) 649V/gain 1.0 and FL3 640V/gain 1.0. A gating strategy on the green fluorescent channel (FL1) was employed to distinguish different subpopulations as described earlier (Prest *et al*., 2013).

To study the adaptation at the population level under continuous low energy flux condition, the cells were harvested from the chemostats at steady state for different D. For determination of total cell concentration, cells were stained with 10 μl mL^{-1} SYBR Green I (1000× stock solution, Invitrogen-Thermo Scientific), and incubated for 13 min at 37°C in darkness before adding reference beads. Green fluorescence was collected in the Fluorescence Channel 1 (FL1 569 nm), and red fluorescence in the Fluorescence Channel 3 (FL3 640 nm), while forward and side scattered light intensities were collected as well. All parameters were collected as logarithmic signals. Microbial cells were distinguished from the reference beads using the forward and side scatter, and from inorganic and organic particles (background noise) using FL1 and FL3. Previous studies have shown that the dot plots of green fluorescence (FL1) against red fluorescence (FL3) are an efficient way to separate the positive signals from the background noise (Gasol *et al*., 1999; Gasol and Del Giorgio, 2000; Hammes and Egli, 2005, 2010). Hence, an electronic gate can be defined in the combined dot/density plots of FL1 against versus FL3 to discriminate the cells efficiently from the background (Supporting Information Fig. S4). Subpopulations – HNA and LNA cells – were analysed in the same run and were distinguished

using the Side Scatter and Fluorescence Channel 1 (FL1 569 nm). More details on this approach for water samples are provided by Gasol *et al*., 1999, Hammes *et al*., 2008 and Prest *et al*., 2013. The proportion of dead cells was estimated via propidium iodide staining, as described in previous studies (Ehrl *et al*., 2019; Kundu *et al*., 2019). The flow cytometry machine was cleaned to remove particulate accumulations before measuring the samples as per the manufacturer's instructions (Beckman Coulter). All the reagents were filtered (0.22 μm). Instead of phosphate buffer saline, IsoFlow™ (Beckman Coulter) was used as a sheath fluid to get a good signal-to-noise ratio. Samples from each biological replicate were measured twice.

Estimation of subpopulations

The measured fluorescence intensity distributions in batch and fed-batch experiments represented as the sum of the two time-dependent distributions $C_g(t)$ and $C_{ng}(t)$ of the 'growing' and 'non-growing' subclass of the population, respectively.

$$C(t) = C_g(t) + C_{ng}(t), \tag{13}$$

where the areas of the $C_g(t)$ and $C_{ng}(t)$ distributions represent the total cell counts N_g and N_{ng}, respectively. The optimum threshold separating the two subclasses of population $C_g(t)$ and $C_{ng}(t)$ was obtained by determining the minima between the two prominent peaks in the distributions. 'peakutils.indexes' function in Python, which identifies prominent peaks by taking the first order difference in a data array was used for this purpose (Oliphant, 2007; Negri and Vestri, 2017). The two areas separated by this threshold were obtained by numerical integration of the respective fraction of data using trapezoidal rule.

In the case of chemostat experiments, HNA and LNA subpopulations were analysed by employing a specific gating strategy by the CXP software. For data visualization, list mode data files were imported on Python platform using Cytoflow package. The log-transformed data were linearized for plotting.

Measurement of atrazine concentration

After filtering the samples, atrazine concentration was measured using a Prominence HPLC system (Shimadzu Corp., Kyoto, Japan) together with a 100 × 4.6 mm Kinetex 5 μm Biphenyl 100 Å column equipped with a SecurityGuard ULTRA Biphenyl cartridge (both Phenomenex Inc., Torrance, CA). Peak separation was achieved by 1 ml/min isocratic flow of 51% 5 mM KH_2PO_4 buffer pH 7% and 49% methanol for 9 min. The compounds were detected by ultraviolet absorbance at 222 nm, and the peaks were quantified using LabSolutions V 5.71 SP2 (Shimadzu Corp.).

Model implementation, calibration and analysis

The model implementation, fitting parameter estimations, and model analysis was performed using Python and employing the built-in functions in scientific libraries NumPy and SciPy (Oliphant, 2007). Equations were integrated and solved at each time step using the Python 3 package SciPy's integration function odeint. The resulting values were added to each respective concentration (biomass, substrate) in the previous time step, which produced dynamics of subpopulations and residual substrate over the cultivation time period respective for each condition. Three kinetic parameters μ_{max}, K_S and q_s^{max} are taken from our previous study (Kundu *et al*., 2019). Endogenous decay (K_d) was estimated as a product of maintenance demand and maximum growth yield, that is, $K_d = (m_s \vee m'_s) \cdot Y_G$. The parameters Υ, δ and ψ were estimated from the experimentally measured N_g and N_{ng} and the residual atrazine concentration (C_s) data by minimizing the Root mean squared error (RMSE) as objective function.

$$\text{RMSE} = \sqrt{\frac{\sum (\vartheta_{exp} - \vartheta_{sim})^2}{N}}. \tag{14}$$

The 'brute force' optimization method was used to find the global minimum of the objective function to compute the objective function at each point of a multidimensional grid of points using lmfit python package (Newville *et al*., 2014). This multidimensional grid contained ranges of Υ (0.004, 0.01), δ (0.001, 0.008) and ψ (0.01, 0.05) with linear grid space of 0.001, 0.001 and 0.005, respectively. Thereafter, the result of 'brute force' minimization was fed as initial guess to obtain a more precise (local) minimum using the downhill simplex algorithm (Nelder and Mead, 1965). The empirical data of residual atrazine concentration, total cell counts, and concentration of LNA and HNA cells from the chemostat cultivation of *A. aurescens* TC1 at D of 0.023 h⁻¹ were used to calibrate the proposed model (Eqs 1, 2 and 7). Furthermore, to quantify the parameter uncertainty on model output, the MCMC technique was applied using emcee, a Python implementation of MCMC algorithm (Goodman and Weare, 2010).

Variance-based global sensitivity analysis (SA) is applied to identify influential model parameters, that is, to more precisely focus on how the input variability influences the model output (Sobol', 1990; Hoeffding, 1992; Homma and Saltelli, 1996; Saltelli, 2002). In this study, Sobol's method (1990) was used to identify the first-order

indices (the contribution to the output variance by a single model input alone) and the second-order indices (the contribution to the output variance by two model inputs). The estimation of Sobol's indices is based on Monte Carlo simulation (sample size of 10,000) to sample over the entire parameter space (Sobol', 1990; Saltelli, 2002). The sampling technique proposed by Saltelli (2002) for Sobol's sensitivity indices was adopted. Sobol's SA was performed using functions built-in SALib (Herman and Usher, 2017) and NumPy Python libraries (Oliphant, 2007).

Acknowledgement

References

Acar, M., Mettetal, J.T., and Van Oudenaarden, A. (2008) Stochastic switching as a survival strategy in fluctuating environments. *Nat Genet* **40**: 471–475.

Ackermann, M. (2015) A functional perspective on phenotypic heterogeneity in microorganisms. *Nat Rev Microbiol* **13**: 497–508.

Akerlund, T., Nordström, K., and Bernander, R. (1995) Analysis of cell size and DNA content in exponentially growing and stationary-phase batch cultures of *Escherichia coli*. *J Bacteriol* **177**: 6791–6797.

Albertson, N.H., Nyström, T., and Kjelleberg, S. (1990) Macromolecular synthesis during recovery of the marine Vibrio sp. S14 from starvation. *Microbiology* **136**: 2201–2207.

Arrieta, J.M., Mayol, E., Hansman, R.L., Herndl, G.J., Dittmar, T., and Duarte, C.M. (2015) Dilution limits dissolved organic carbon utilization in the deep ocean. *Science* **348**: 331–333.

Balaban, N.Q., Merrin, J., Chait, R., Kowalik, L., and Leibler, S. (2004) Bacterial persistence as a phenotypic switch. *Science* **305**: 1622–1625.

Bayer, A., Drexel, R., Weber, N., and Griebler, C. (2016) Quantification of aquatic sediment prokaryotes – a multiple-steps optimization testing sands from pristine and contaminated aquifers. *Limnol Manag Inl Waters* **56**: 6–13.

Bernard, L., Courties, C., Servais, P., Troussellier, M., Petit, M., and Lebaron, P. (2000) Relationships among bacterial cell size, productivity, and genetic diversity in aquatic environments using cell sorting and flow cytometry. *Microb Ecol* **40**: 148–158.

Boer, V.M., Crutchfield, C.A., Bradley, P.H., Botstein, D., and Rabinowitz, J.D. (2010) Growth-limiting intracellular metabolites in yeast growing under diverse nutrient limitations. *Mol Biol Cell* **21**: 198–211.

Bouvier, T., Del Giorgio, P.A., and Gasol, J.M. (2007) A comparative study of the cytometric characteristics of high and low nucleic-acid bacterioplankton cells from different aquatic ecosystems. *Environ Microbiol* **9**: 2050–2066.

Boylen, C.W., and Mulks, M.H. (1978) The survival of coryneform bacteria during periods of prolonged nutrient starvation. *Microbiology* **105**: 323–334.

Bremer, H., and Dennis, P.P. (1996) Modulation of chemical composition and other parameters of the cell by growth rate. *E coli Salmonella Cell Mol Biol* **2**: 1553–1569.

Cooper, S., and Helmstetter, C.E. (1968) Chromosome replication and the division cycle of *Escherichia coli* Br. *J Mol Biol* **31**: 519–540.

Egli, T. (2010) How to live at very low substrate concentration. *Water Res* **44**: 4826–4837.

Ehrl, B.N., Kundu, K., Gharasoo, M., Marozava, S., and Elsner, M. (2019) Rate-limiting mass transfer in micropollutant degradation revealed by isotope fractionation in chemostat. *Environ Sci Technol* **53**: 1197–1205.

Elowitz, M.B., Levine, A.J., Siggia, E.D., and Swain, P.S. (2002) Stochastic gene expression in a single cell. *Science* **297**: 1183–1186.

Ercan, O., Bisschops, M.M.M., Overkamp, W., Jørgensen, T. R., Ram, A.F., Smid, E.J., *et al*. (2015) Physiological and transcriptional responses of different industrial microbes at near-zero specific growth rates. *Appl Environ Microbiol* **81**: 5662–5670.

Fida, T.T., Moreno-Forero, S.K., Heipieper, H.J., and Springael, D. (2013) Physiology and transcriptome of the polycyclic aromatic hydrocarbon-degrading Sphingomonas sp. LH128 after long-term starvation. *Microbiology* **159**: 1807–1817.

Finkel, S.E. (2006) Long-term survival during stationary phase: evolution and the GASP phenotype. *Nat Rev Microbiol* **4**: 113–120.

Finkel, S.E., and Kolter, R. (1999) Evolution of microbial diversity during prolonged starvation. *Proc Natl Acad Sci* **96**: 4023–4027.

Franchini, A.G., and Egli, T. (2006) Global gene expression in *Escherichia coli* K-12 during short-term and long-term adaptation to glucose-limited continuous culture conditions. *Microbiology* **152**: 2111–2127.

Garland, T., and Kelly, S.A. (2006) Phenotypic plasticity and experimental evolution. *J Exp Biol* **209**: 2344–2361.

Gasol, J.M., and Del Giorgio, P.A. (2000) Using flow cytometry for counting natural planktonic bacteria and understanding the structure of planktonic bacterial communities. *Sci Mar* **64**: 197–224.

Gasol, J.M., Zweifel, U.L., Peters, F., Fuhrman, J.A., and Hagström, Å. (1999) Significance of size and nucleic acid content heterogeneity as measured by flow cytometry in natural planktonic bacteria. *Appl Environ Microbiol* **65**: 4475–4483.

Goodman, J., and Weare, J. (2010) Ensemble samplers with affine invariance. *Commun Appl Math Comput Sci* **5**: 65–80.

Gray, D.A., Dugar, G., Gamba, P., Strahl, H., Jonker, M.J., and Hamoen, L.W. (2019) Extreme slow growth as alternative strategy to survive deep starvation in bacteria. *Nat Commun* **10**: 890.

Griebler, C., and Lueders, T. (2009) Microbial biodiversity in groundwater ecosystems. *Freshw Biol* **54**: 649–677.

Griebler, C., Mindl, B., and Slezak, D. (2001) Combining DAPI and SYBR Green II for the enumeration of total

bacterial numbers in aquatic sediments. *Int Rev Hydrobiol A J Cover all Asp Limnol Mar Biol* **86**: 453–465.

Hammes, F., Berney, M., Wang, Y., Vital, M., Köster, O., and Egli, T. (2008) Flow-cytometric total bacterial cell counts as a descriptive microbiological parameter for drinking water treatment processes. *Water Res* **42**: 269–277.

Hammes, F., and Egli, T. (2010) Cytometric methods for measuring bacteria in water: advantages, pitfalls and applications. *Anal Bioanal Chem* **397**: 1083–1095.

Hammes, F.A., and Egli, T. (2005) New method for assimilable organic carbon determination using flow-cytometric enumeration and a natural microbial consortium as inoculum. *Environ Sci Technol* **39**: 3289–3294.

Hartke, A., Giard, J.-C., Laplace, J.-M., and Auffray, Y. (1998) Survival of *Enterococcus faecalis* in an oligotrophic microcosm: changes in morphology, development of general stress resistance, and analysis of protein synthesis. *Appl Environ Microbiol* **64**: 4238–4245.

Heijnen J.J. (1999) Bioenergetics of microbial growth. In *Bioprocess Technology: Fermentation, Biocatalysis and Separation*. Flickinger C.M., and Drew C.W. (eds). New York: Wiley, pp. 267–291.

Herman, J., and Usher, W. (2017) SALib: an open-source Python library for sensitivity analysis. *J Open Source Softw* **2**: 97.

Hoeffding, W. (1992) A class of statistics with asymptotically normal distribution. In *Breakthroughs in Statistics*, New York: Springer, pp. 308–334.

Hoehler, T.M., and Jørgensen, B.B. (2013) Microbial life under extreme. *Nat Rev Microbiol* **11**: 83–94.

Holmquist, L., and Kjelleberg, S. (1993) The carbon starvation stimulon in the marine *Vibrio* sp. S14 (CCUG 15956) includes three periplasmic space protein responders. *Microbiology* **139**: 209–215.

Homma, T., and Saltelli, A. (1996) Importance measures in global sensitivity analysis of nonlinear models. *Reliab Eng Syst Saf* **52**: 1–17.

Ihssen, J., and Egli, T. (2004) Specific growth rate and not cell density controls the general stress response in *Escherichia coli*. *Microbiology* **150**: 1637–1648.

Jones, S.E., and Lennon, J.T. (2010) Dormancy contributes to the maintenance of microbial diversity. *Proc Natl Acad Sci* **107**: 5881–5886.

Kelly, S.A., Panhuis, T.M., and Stoehr, A.M. (2011) Phenotypic plasticity: molecular mechanisms and adaptive significance. *Compr Physiol* **2**: 1417–1439.

Kempes, C.P., van Bodegom, P.M., Wolpert, D., Libby, E., Amend, J., and Hoehler, T. (2017) Drivers of bacterial maintenance and minimal energy requirements. *Front Microbiol* **8**: 31.

Kjelleberg, S., Albertson, N., Flärdh, K., Holmquist, L., Jouper-Jaan, Å., Marouga, R., *et al*. (1993) How do non-differentiating bacteria adapt to starvation? *Antonie Van Leeuwenhoek* **63**: 333–341.

Klumpp, S., Zhang, Z., and Hwa, T. (2009) Growth rate-dependent global effects on gene expression in bacteria. *Cell* **139**: 1366–1375.

Konopka, A. (1999) Theoretical analysis of the starvation response under substrate pulses. *Microb Ecol* **38**: 321–329.

Konopka, A., Zakharova, T., Oliver, L., Camp, D., and Turco, R.F. (1996) Biodegradation of organic wastes containing surfactants in a biomass recycle reactor. *Appl Environ Microbiol* **62**: 3292–3297.

Kotte, O., Volkmer, B., Radzikowski, J.L., and Heinemann, M. (2015) Phenotypic bistability in *Escherichia coli*'s central carbon metabolism phenotypic bistability in *Escherichia coli*'s central carbon metabolism. *Mol Syst Biol* **10**: 1–11.

Kundu, K., Marozava, S., Ehrl, B., Merl-Pham, J., Griebler, C., and Elsner, M. (2019) Defining lower limits of biodegradation: atrazine degradation regulated by mass transfer and maintenance demand in *Arthrobacter aurescens* TC1. *The ISME Journal* **13**: 2236–2251.

Lebaron, P., Servais, P., Agogué, H., Courties, C., and Joux, F. (2001a) Does the high nucleic acid content of individual bacterial cells allow us to discriminate between active cells and inactive cells in aquatic systems? *Appl Environ Microbiol* **67**: 1775–1782.

Lebaron, P., Servais, P., Baudoux, A.-C., Bourrain, M., Courties, C., and Parthuisot, N. (2002) Variations of bacterial-specific activity with cell size and nucleic acid content assessed by flow cytometry. *Aquat Microb Ecol* **28**: 131–140.

Lebaron, P., Servais, P., Troussellier, M., Courties, C., Muyzer, G., Bernard, L., *et al*. (2001b) Microbial community dynamics in Mediterranean nutrient-enriched seawater mesocosms: changes in abundances, activity and composition. *FEMS Microbiol Ecol* **34**: 255–266.

Lennon, J.T., and Jones, S.E. (2011) Microbial seed banks: the ecological and evolutionary implications of dormancy. *Nat Rev Microbiol* **9**: 119–130.

Lever, M.A., Rogers, K.L., Lloyd, K.G., Overmann, J., Schink, B., Thauer, R.K., *et al*. (2015) Life under extreme energy limitation: a synthesis of laboratory- and field-based investigations. *FEMS Microbiol Rev* **39**: 688–728.

Lewis, K. (2007) Persister cells, dormancy and infectious disease. *Nat Rev Microbiol* **5**: 48–56.

Li, W.K.W., Jellett, J.F., and Dickie, P.M. (1995) DNA distributions in planktonic bacteria stained with TOTO or TO-PRO. *Limnol Oceanogr* **40**: 1485–1495.

Losick, R., and Desplan, C. (2008) Stochasticity and cell fate. *Science* **320**: 65–68.

Mellage, A., Eckert, D., Grösbacher, M., Inan, A.Z., Cirpka, O. A., and Griebler, C. (2015) Dynamics of suspended and attached aerobic toluene degraders in small-scale flow-through sediment systems under growth and starvation conditions. *Environ Sci Technol* **49**: 7161–7169.

Morita, R.Y. (1997) *Bacteria in Oligotrophic Environments: Starvation-Survival Lifestyle*. New York, NY: Chapman & Hall.

Nair, S., and Finkel, S.E. (2004) Dps protects cells against multiple stresses during stationary phase. *J Bacteriol* **186**: 4192–4198.

Negri, L.H. and Vestri, C. (2017) *Lucashn/Peakutils: v1.1.0*. (Version v1.1.0). Zenodo. http://doi.org/10.5281/zenodo.887917.

Neidhardt, F.C., Ingraham, J.L., and Schaechter, M. (1990) *Physiology of the Bacterial Cell: A Molecular Approach*. Sunderland, MA: Sinauer Associates.

Nelder, J.A., and Mead, R. (1965) A simplex method for function minimization. *Comput J* **7**: 308–313.

Newville, M., Stensitzki, T., Allen, D.B., Rawlik, M., Ingargiola, A., and Nelson, A. (2014) LMFIT: non-linear least-square minimization and curve-fitting for Python. *Zenodo*. https://doi.org/10.5281/zenodo.11813.

Nishimura, Y., and Bailey, J.E. (1981) Bacterial population dynamics in batch and continuous-flow microbial reactors. *AIChE J* **27**: 73–81.

Oliphant, T.E. (2007) Python for scientific computing. *Comput Sci Eng* **9**: 10–20.

Philippi, T., and Seger, J. (1989) Hedging one's evolutionary bets, revisited. *Trends Ecol Evol* **4**: 41–44.

Pirt, S.J. (1982) Maintenance energy: a general model for energy-limited and energy-sufficient growth. *Arch Microbiol* **133**: 300–302.

Prest, E.I., Hammes, F., Kötzsch, S., Van Loosdrecht, M.C.M., and Vrouwenvelder, J.S. (2013) Monitoring microbiological changes in drinking water systems using a fast and reproducible flow cytometric method. *Water Res* **47**: 7131–7142.

Proctor, C.R., Besmer, M.D., Langenegger, T., Beck, K., Walser, J.-C., Ackermann, M., *et al*. (2018) Phylogenetic clustering of small low nucleic acid-content bacteria across diverse freshwater ecosystems. *ISME J* **12**: 1344–1359.

Rappé, M.S., Connon, S.A., Vergin, K.L., and Giovannoni, S. J. (2002) Cultivation of the ubiquitous SAR11 marine bacterioplankton clade. *Nature* **418**: 630–633.

Raser, J.M., and O'shea, E.K. (2005) Noise in gene expression: origins, consequences, and control. *Science* **309**: 2010–2013.

Roller, B.R.K., Stoddard, S.F., and Schmidt, T.M. (2016) Exploiting rRNA operon copy number to investigate bacterial reproductive strategies. *Nat Microbiol* **1**: 16160.

Rubbens, P., Schmidt, M.L., Props, R., Biddanda, B.A., Boon, N., Waegeman, W., and Denef, V.J. (2019) Randomized lasso links microbial taxa with aquatic functional groups inferred from flow cytometry. *MSystems* **4**: e00093-19.

Saltelli, A. (2002) Making best use of model evaluations to compute sensitivity indices. *Comput Phys Commun* **145**: 280–297.

Schattenhofer, M., Wulf, J., Kostadinov, I., Glöckner, F.O., Zubkov, M.V., and Fuchs, B.M. (2011) Phylogenetic characterisation of picoplanktonic populations with high and low nucleic acid content in the North Atlantic Ocean. *Syst Appl Microbiol* **34**: 470–475.

Schreiber, F., Littmann, S., Lavik, G., Escrig, S., Meibom, A., Kuypers, M.M.M., and Ackermann, M. (2016) Phenotypic heterogeneity driven by nutrient limitation promotes growth in fluctuating environments. *Nat Microbiol* **1**: 16055.

Sekhar, A., Horemans, B., Aamand, J., Sørensen, S.R., Vanhaecke, L., Vanden Bussche, J., *et al*. (2016) Surface colonization and activity of the 2,6-dichlorobenzamide (BAM) degrading *Aminobacter* sp. strain MSH1 at macro- and micropollutant BAM concentrations. *Environ Sci Technol* **50**: 10123–10133.

Servais, P., Casamayor, E.O., Courties, C., Catala, P., Parthuisot, N., and Lebaron, P. (2003) Activity and diversity of bacterial cells with high and low nucleic acid content. *Aquat Microb Ecol* **33**: 41–51.

Sherr, E.B., Sherr, B.F., and Longnecker, K. (2006) Distribution of bacterial abundance and cell-specific nucleic acid content in the Northeast Pacific Ocean. *Deep Sea Res Part I Oceanogr Res Pap* **53**: 713–725.

Sobol', I.M. (1990) On sensitivity estimation for nonlinear mathematical models. *Mat Model* **2**: 112–118.

Stolpovsky, K., Martinez-Lavanchy, P., Heipieper, H.J., Van Cappellen, P., and Thullner, M. (2011) Incorporating dormancy in dynamic microbial community models. *Ecol Model* **222**: 3092–3102.

Stouthamer, A.H., Bulthuis, B.A., Van Verseveld, H.W., Bazin, M.J., Poole, M.J., and Keevil, R.K. (1990) Energetics of growth at low growth rates and its relevance for the maintenance concept. *Microb growth Dyn* **28**: 85–102.

Strong, L.C., Rosendahl, C., Johnson, G., Sadowsky, M.J., and Wackett, L.P. (2002). *Arthrobacter aurescens* TC1 metabolizes diverse s-sriazine ring compounds. *Appl Environ Microbiol* **68**: 5973–5980.

Trautwein, K., Lahme, S., Wöhlbrand, L., Feenders, C., Mangelsdorf, K., Harder, J., *et al*. (2012) Physiological and proteomic adaptation of 'Aromatoleum aromaticum' EbN1 to low growth rates in benzoate-limited, anoxic chemostats. *J Bacteriol* **194**: 2165–2180.

Van Bodegom, P. (2007) Microbial maintenance: a critical review on its quantification. *Microb Ecol* **53**: 513–523.

Vila-Costa, M., Gasol, J.M., Sharma, S., and Moran, M.A. (2012) Community analysis of high-and low-nucleic acid-containing bacteria in NW Mediterranean coastal waters using 16S rDNA pyrosequencing. *Environ Microbiol* **14**: 1390–1402.

Wallace, P.K., Tario, J.D., Jr., Fisher, J.L., Wallace, S.S., Ernstoff, M.S., and Muirhead, K.A. (2008) Tracking antigen-driven responses by flow cytometry: monitoring proliferation by dye dilution. *Cytom Part A* **73**: 1019–1034.

Wang, G., Mayes, M.A., Gu, L., and Schadt, C.W. (2014) Representation of dormant and active microbial dynamics for ecosystem modeling. *PLoS One* **9**: e89252.

Wang, Y., Hammes, F., Boon, N., Chami, M., and Egli, T. (2009) Isolation and characterization of low nucleic acid (LNA)-content bacteria. *ISME J* **3**: 889–902.

Westerberg, K., Elväng, A.M., Stackebrandt, E., and Jansson, J.K. (2000) *Arthrobacter chlorophenolicus* sp. nov., a new species capable of degrading high concentrations of 4-chlorophenol. *Int J Syst Evol Microbiol* **50**: 2083–2092.

Wick, L.M., Quadroni, M., and Egli, T. (2001) Short-and long-term changes in proteome composition and kinetic properties in a culture of *Escherichia coli* during transition from glucose-excess to glucose-limited growth conditions in continuous culture and vice versa. *Environ Microbiol* **3**: 588–599.

Zinser, E.R., and Kolter, R. (2000) Prolonged stationary-phase incubation selects forlrp mutations in *Escherichia coli* K-12. *J Bacteriol* **182**: 4361–4365.

Zinser, E.R., and Kolter, R. (2004) *Escherichia coli* evolution during stationary phase. *Res Microbiol* **155**: 328–336.

Zubkov, M.V., Fuchs, B.M., Burkill, P.H., and Amann, R. (2001) Comparison of cellular and biomass specific activities of dominant bacterioplankton groups in stratified waters of the Celtic Sea. *Appl Environ Microbiol* **67**: 5210–5218.

Zubkov, M.V., Fuchs, B.M., Tarran, G.A., Burkill, P.H., and Amann, R. (2002) Mesoscale distribution of dominant

bacterioplankton groups in the northern North Sea in early summer. *Aquat Microb Ecol* **29**: 135–144.

Supporting Information

Additional Supporting Information may be found in the online version of this article at the publisher's web-site:

Data S1. Model analysis

Figure S1. Traces of MCMC chain for each estimated parameter over 350,0000 iterations for *Arthrobacter aurescens* TC1. In f denotes the logarithm of the substrate concentration, that is, C_s

Figure S2. Corner plot showing the posterior distribution of the model parameters through MCMC sampling. The marginal distribution of the parameters is provided on the diagonal along with the median (blue line). The off-diagonal plots show the joint distribution of each pair of parameters and the blue lines are the true values used to simulate the data

Figure S3. First order (S1), total order (ST) and second order (S2) Sobol' indices for all model parameters on residual 'non-growing' biomass concentration in chemostat. Most influential parameters have higher variance. The error bar represents the confidence intervals based on 10,0000 bootstrap samples

Figure S4. Data collection and gating strategy for flow cytometry analysis. (A) Forward scatter (FS) vs side scatter (SS) allows to distinguish between stained cells and reference beads. (B) Selection of bacteria using a fixed gate on the green (FL3)/red fluorescence (FL1) density plot for exclusion of background. (C) Selection of low and high nucleic acid content (LNA and HNA) bacteria on the resulting green fluorescence of selected data (from panel B) vs side scatter. The data is log-transformed

Figure S5. Dynamic total biomass, 'growing' (HNA) and 'non-growing' (LNA) biomass; and substrate, atrazine concentration in the chemostats under varying energy flux controlled by dilution rates. Solid lines depict the model prediction (eqs 1, 2 and 7), whereas the markers show the experimental data (unfilled markers indicate data points used for model calibration). Data is from one biological replicate

Table S1. Conditions of chemostat cultivations of *Arthrobacter aurescens* TC1

Table S2. Range of values of kinetic parameters used in sensitivity analysis